Investigation of valence orbitals of propene by electron momentum spectroscopy

C. G. Ning, X. G. Ren, J. K. Deng,[a] S. F. Zhang, G. L. Su, F. Huang, and G. Q. Li
Department of Physics, Tsinghua University, Beijing 100084, People's Republic of China

(Received 9 December 2004; accepted 13 April 2005; published online 10 June 2005)

The binding energy spectra and momentum distributions of all valence orbitals of propene were studied by electron momentum spectroscopy (EMS) as well as Hartree–Fock and density functional theoretical calculations. The experiment was carried out at impact energies of 1200 eV and 600 eV on the state-of-the-art EMS spectrometer developed at Tsinghua University recently. The experimental momentum profiles of the valence orbitals were obtained and compared with the various theoretical calculations. Moreover, the experiment with a new analysis method presents a strong support for the correct ordering of the orbital $8a'$ and $1a''$, i.e., $9a'<8a'<1a''<7a'$. © *2005 American Institute of Physics*. [DOI: 10.1063/1.1926285]

I. INTRODUCTION

A detailed knowledge of molecular electronic structure, particularly in the outer valence orbitals, is a key factor in understanding chemical properties including reactivity. Electron momentum spectroscopy (EMS) can provide a direct imaging of the electron density for each individual orbital in momentum space. These EMS experiments, together with appropriate Hartree–Fock (HF) or density functional theory (DFT) quantum mechanical calculations, have been able to provide detailed quantitative information on the reactive parts (i.e., the valence orbitals) of molecular electron densities. EMS has been shown to be a powerful and informative experimental tool for study of the electronic structure of atoms, molecules, biomolecules, and condensed matter.[1–3] It can access the complete valence shell binding energy range, though with lower energy resolution than in most photoelectron spectroscopy (PES) studies. It should be noted that EMS is particularly sensitive to the low momentum (large r) part of the orbital densities that may be important in molecular recognition and the initial process involved in the early stages of a chemical reaction. According to Fourier transform theory, the momentum distribution is equivalent to position distribution. Cooper *et al.*[4,5] have shown that assessment of electron density topographies is even more important for molecular carried out in momentum space than in the more commonly used position space.

Propene, C_3H_6, as the simplest straight chain hydrocarbon molecule that has both carbon-carbon double bond and carbon-carbon single bond, serves as an excellent prototype of model alkene. In addition to its fundamental interest in quantum chemistry, propene is also an important raw material for reagent compound synthesis and polymer production. The electronic states of propene were extensively investigated by various experimental and theoretical methods.[6–9] However, to the best of our knowledge, no electron momentum spectroscopic study on this molecule has ever been reported.

Another motivation of the present work is that the ordering of the outer valence molecular orbitals $8a'$ and $1a''$ still remains ambiguous. According to earlier He I and He II PES,[6,7] the ordering was $9a'<1a''<8a'<7a'$, while more recently Bawagan *et al.*[9] found them to $9a'<8a'<1a''<7a'$. EMS can provide a unique way of unambiguous experimental assignment of molecular orbitals by simply comparing the experimental momentum profiles with theoretical calculations.[10–13] In the present work, we report the EMS study of propene at impact energies of 600 eV and 1200 eV. The experimental momentum profiles of the valence orbitals were obtained and compared with various theoretical calculations. Ambiguities regarding the ordering of these states have been resolved.

II. EXPERIMENTAL METHODS AND THEORETICAL BACKGROUND

Recently we have developed a new type of EMS spectrometer with two orders higher efficiency than our previous one.[14] The basic principle of EMS is ionization reaction initiated by electron collision, i.e., the $(e,2e)$ reaction. The gas-phase target molecules are ionized by impact with a high energy electron beam. The outgoing electrons (scattered and ionized) are angle and energy selected and then detected in coincidence. The experimental geometry is symmetric noncoplanar, i.e., the two outgoing electrons are selected to have equal polar angles $(\theta_1=\theta_2=45°)$ relative to the incoming electron beam direction. The azimuthal angles ϕ (angle between the outgoing electron direction in the plane normal to the beam direction, and $\phi=0$ is the scattering plane) from $-38°$ to $38°$ are simultaneously measured, which is the significant improvement compared with our previous spectrometer which only collects $(e,2e)$ events at a fixed ϕ angle one time. A profile of differential cross section versus recoil

[a]Author to whom correspondence should be addressed. Electronic mail: djk-dmp@mail.tsinghua.edu.cn

momentum for each energy resolved state of the target molecules can be obtained from these binding energy spectra of different ϕ angles. Under the binary encounter requirements of high impact energy and high momentum transfer, the initial momentum p of the knocked-out electron is related to the azimuthal angle by

$$p = \{(2p_1 \cos\theta_1 - p_0)^2 + [2p_1 \sin\theta_1 \sin(\phi/2)]^2\}^{1/2}, \quad (1)$$

where $p_1, p_2 (p_1 = p_2)$ are the magnitude of the momentum of each of the two outgoing electron and p_0 is the momentum of the incident electron.

The EMS binary $(e,2e)$ differential cross section in the plane wave impulse approximation for randomly oriented gas-phase molecules is given by[1]

$$\sigma_{\mathrm{EMS}} \propto \int \frac{d\Omega}{4\pi} |\langle p\psi_f^{N-1} | \psi_i^N \rangle|^2, \quad (2)$$

where p is the momentum of the target electron prior to the electron ejection. $|\Psi_f^{N-i}\rangle$ and $|\Psi_i^N\rangle$ are the total electronic wave functions for the final ion state and the target molecule ground (initial) state, respectively. Equation (2) can be greatly simplified by using the target Hartree–Fock approximation (THFA). Within the THFA, only final (ion) state correlation is allowed and the many-body wave functions $|\Psi_f^{N-1}\rangle$ and $|\Psi_i^N\rangle$ are approximated as independent particle determinants of ground state target Hartree–Fock orbital. In this approximation Eq. (1) is reduced to[1]

$$\sigma_{\mathrm{EMS}} \propto S_i^f \int d\Omega |\psi_j(p)|^2, \quad (3)$$

where $|\psi_j(p)\rangle$ is the one-electron momentum space canonical Hartree–Fock orbital wave function for the jth electron, corresponding to the orbital from which the electron was ionized, S_i^f is the spectroscopic factor (also known as the pole strength), the probability of the ionization event producing a one-hole configuration of the final ion state. The quantity $|\psi_j(p)\rangle$ is the Fourier transform of the more familiar one-electron position space orbital wave function $|\psi_j(r)\rangle$. The integral in Eq. (3) is known as the spherically averaged one-electron momentum distribution. Within this approximation EMS has the ability to image the electron density distribution in individual orbitals selected according to their binding energies.

The Kohn–Sham DFT reinterprets Eq. (2) by an alternative approach,[15] and it gives a result similar to Eq. (3) with the canonical Hartree–Fock orbital replaced by a momentum space Kohn–Sham orbital $|\psi_j^{\mathrm{KS}}(p)\rangle$,

$$\sigma_{\mathrm{EMS}} \propto S_j^f \int d\Omega |\psi_j^{\mathrm{KS}}(p)|^2. \quad (4)$$

It should be noted that the electron correlation effects in the target ground state are included in the target Kohn–Sham approximation via the exchange correlation potential, so, in some manners, Kohn–Sham orbital can be regarded as a Hartree–Fock method corrected for the correlation effects.

With our recently developed EMS spectrometer, binding energy spectra (BES) are collected at a range of azimuthal ϕ angles simultaneously. Electron density distributions as a function of angle ϕ are obtained by deconvolution of these binding energy spectra using Gaussian functions located at each ionization energy in the BES. The widths of the Gaussian functions can be determined from a consideration of published PES vibronic manifolds and the instrumental energy resolution function [1.2 eV full width at half maximum (FWHM)]. For each ionization process, the area of fitted peak is plotted as a function of momentum [calculated from ϕ by Eq. (1)]. The set of areas as a function of momentum for a specific binding energy is referred to as an experimental momentum profile (XMP). To compare the XMPs with the relative cross sections calculated as a function of momentum using expressions (2)–(4) above, the effects of the finite spectrometer acceptance angles in both θ and ϕ ($\Delta\theta \approx \pm 0.7°$ and $\Delta\phi \approx \pm 1.9°$) must be included. This is achieved in the present work by the Gaussian method.[16]

Propene has C_s point group symmetry and its electronic configuration in the ground state can be written as

$$(\mathrm{core})^6 \underbrace{(4a')^2(5a')^2(6a')^2}_{\text{inner valence}} \underbrace{(7a')^2(1a'')^2(8a')^2(9a')^2(10a')^2(2a'')^2}_{\text{outer valence}}.$$

In the ground state, the 24 electrons are arranged in 12 double-occupied orbitals in the independent particle description. All the molecular orbitals are either A' or A'' symmetry. The PES of propene has been investigated extensively both experimentally and theoretically, such as He I PES, He II PES, x-ray PES, and synchrotron radiation PES reported by Refs. 6–9, respectively. The assignment of the order of occupation for these valence orbitals, both from the PES experiments and the molecular orbital calculations, has been discussed in Refs. 17 and 9. Peak ordering of $8a'$ and $1a''$ is reversed in the theoretical calculations in Refs. 6–8, while more accurate multireference singles and doubles configuration interaction (MRSDCI) theoretical calculation gave the ordering as shown above.[9] This will be discussed in a later section.

The gaseous sample of propene measured in this work was 99.5% of purity, and was used directly without further purification.

III. RESULTS AND DISCUSSION

A. Binding energy spectra

The EMS spectrometer used in this work is not only an energy multichannel but also an angle multichannel. Compared with our previous one, it detects the $(e,2e)$ events with

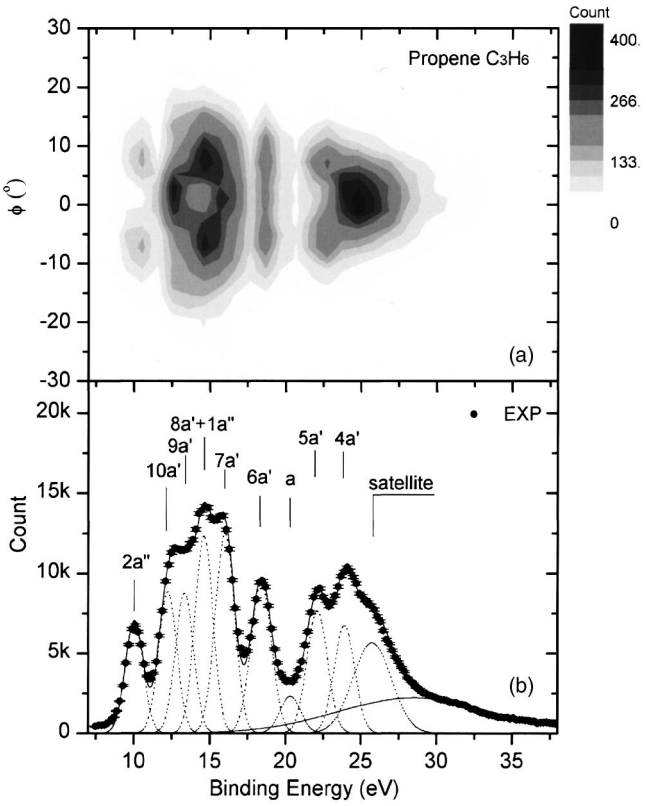

FIG. 1. Binding energy spectra of propene, (a) angle resolved energy map and (b) summed over all ϕ angles, obtained at an impact energy of 1200 eV plus binding energy. The dashed lines represent Gaussian fits to the peaks and the solid curve is the summed fit.

a wider ϕ angle range from −38° to 38° simultaneously, so the detect efficiency is much higher. The typical measurement period is only several hours, while the previous one needs about a month. The angle resolved binding energy spectra is shown in Fig. 1. Just with a glance, one can immediately know the characteristics of each orbital. When summing over all ϕ angles on the map Fig. 1(a), the total energy spectra can be obtained as illustrated in Fig. 1(b). To obtain the experimental momentum profiles, the map is divided into many groups according to the ϕ angle with a step of 1°. The binding energy spectra were fitted with a series of individual Gaussian peaks whose widths are combinations of the EMS instrumental energy resolution and the corresponding Franck–Condon widths derived from high-resolution PES data. Their energy values are given by the ionization energies determined by the high-resolution PES. The fitted Gaussian curves for individual peaks are indicated by dotted lines while their overall fitted spectra are represented by the solid lines in Fig. 1(b). Since the energy separation between $8a'$ and $1a''$ is only 0.52 eV, an averaged ionization potential of $8a'+1a''$ was determined to be 14.6 eV. Some spectroscopic strength with energy higher than 25 eV was observed, and two Gaussian peaks with much broader FWHM were used to approximate their sum intensity. It is due to that there are many satellite peaks with a smaller energy separation at this energy region, and EMS cannot resolve them well. The spectroscopic strength above 25 eV is mainly due to correlation effects in the target or in the final state of residual ion. Moreover, to describe well the experimental binding energy spectra, the Gaussian peak at 20.3 eV indicated by *a* must be included, otherwise the experimental intensity at the region of around 20.3 eV will be greatly underestimated. Satellite-a was also identified by MRSDCI calculation in Ref. 9. The differences of FWHMs of these peaks are due to the vibrational broadening of the lines.

The experimental and theoretical ionization potentials for each valence orbital are compared in Table I. HF and DFT calculations assign a same ordering of $8a''$ and $1a'$ as that of He I and He II PES, while outer-valence Green's function (OVGF) and MRSDCI give the reversed one.

TABLE I. Valence ionization potentials (eV) of propene.

Orbital	PES	EMS[a,b]	HF[a]	DFT[a]	OVGF[a]	MRSDCI[c]
$2a''$	10.03[d]	10.03(0.789±0.010)	9.64	7.06	9.64(0.915)	10.03(0.791)
$10a'$	12.31[d]	12.3(0.998±0.016)	13.31	9.55	12.29(0.908)	12.31(0.806)
$9a'$	13.23[d]	13.2(0.992±0.019)	14.19	10.18	13.19(0.913)	13.27(0.810)
$8a'$	14.48[d]	14.6(0.890±0.011)[e,f]	15.69	11.45	14.48(0.899)	14.67(0.787)
$1a''$	15.0[c]		15.494	11.37	14.60(0.910)	15.22(0.768)
$7a'$	15.9[c]	15.9(0.890±0.011)[f]	17.27	12.73	15.88(0.879)	16.13(0.741)
$6a'$	18.4[c]	18.4(0.752±0.009)	20.53	15.12	18.64(0.852)	19.05(0.516)
$5a'$	22.1[c]	22.1(0.523±0.006)	25.22	18.61		23.69(0.298)
$4a'$	23.9[c]	23.9(0.330±0.008)	28.75	21.34		26.17(0.130)28.00(0.126)
Peak *a*	20.3[c]	20.3(0.174±0.009)				20.43(0.023)

[a]Present work. The basis sets for theoretical calculations are HF/6-311++G**, DFT-B3LYP/6-311++G**, and OVGF/6-311++G**, respectively. OVGF calculation gives the same ordering of $4a'$ and $5a'$ as MRSDCI method, while HF and DFT present a reversed one. The digits in parentheses are the pole strengths. See text for the method about the experimental pole strength obtained by EMS.
[b]The digits in parentheses are the measured pole strengths. The measure errors are estimate from Eq. (7).
[c]Reference 9. For $4a'$, $5a'$, the correlation effects are severe such that the primary peak assignments are tenuous at best. See Ref. 9 for details. The digits in parentheses are the calculated pole strengths.
[d]Reference 6. The ordering of $8a'$, $1a''$ was reversed therein.
[e]Our EMS spectrometer cannot resolve $8a'$ and $1a''$ states, so an averaged binding energy was assigned.
[f]Since $8a'+1a''+7a'$ calculations better describe the experimental distribution, so an averaged pole strength was assigned.

Among all these calculations, OVGF calculations presented more consistent ionization potentials with experiments through all the outer-valence orbitals.

B. Normalization and pole strength

The differential cross sections experimentally obtained by EMS are not absolute, so the obtained relative magnitude needs to be normalized by an absolute scale. Previous literatures[18,11] usually summed the experimental flux at all measured ϕ angles for all the outer-valence states, and then normalizing this to the corresponding sum for the result of the calculation. This method assumed that the outer-valence orbitals' pole strengths were equal to one. However, OVGF and MRSDCI calculations indicated that pole strengths of the outer-valence states are usually not one. Here, we attempt to present a more reasonable method to calculate the pole strengths. If the measured energy range includes all valence states and all corresponding satellite peaks, we have

$$\sum_k \sum_{p_j=0}^{\infty} \frac{1}{\mathrm{eff}(\varepsilon_k,p_j)} I'_k(p_j) p_j^2 \Delta p_j = N \sum_i \int_0^{\infty} \rho_i(p) p^2 dp, \quad (5)$$

where p is the momentum and $\rho(p)$ is the electron density distribution at the momentum space. On the right side of Eq. (5), the integral of the normalized theoretical momentum distribution equals

$$\int_0^{\infty} \rho_l(p) p^2 dp = \frac{1}{4\pi}. \quad (6)$$

The index i represents the ith valence orbital, so the total valence intensities are obtained by summing over i. N is the normalizing number, which will be used for comparing the experimental data with the calculated one. On the left side of Eq. (5), the primed signs represent the experimental measured ones. $\mathrm{eff}(\varepsilon_k,p_j)$ is the response function of the spectrometer at binding energy ε_k and momentum p_j. $I'_k(p_j)$ is the measured intensity distribution of momentum at binding energy ε_k. The index k represents the kth peak on the binding energy spectra, thus the total experimental intensity is obtained by summing over k. Since the measured range of momentum could not reach all momentum space, i.e., from 0 to ∞, the bounds of sum and integral are replaced with practical experimental ranges from $p_{\min}$ to $p_{\max}$, so Eq. (5) is rewritten as

$$\sum_k \sum_{p_j=p_{\min}}^{p_{\max}} \frac{1}{\mathrm{eff}(\varepsilon_k,p_j)} I'_k(p_j) p^2 \Delta p_j = N \sum_{\mathrm{i}} \int_{p_{\min}}^{p_{\max}} \rho_i(p) p^2 dp. \quad (7)$$

For propene, at an impact energy of 1200 eV plus binding energies, $p_{\min} \approx 0.06$ a.u. and $p_{\max} \approx 2.40$ a.u., the integral is about 5% less than the full momentum space integral. It should be noted that the integrals over 0 to $p_{\min}$ are almost ignorable compared with the total integral for each valence orbital, and the integrals over $p_{\max}$ to ∞ are almost same, so the pole strengths calculated by this method are reasonable and quite accurate. The experimental pole strengths for each orbital in Table I are obtained by this method at an impact energy of 1200 eV plus binding energies. It can be seen that it is in good agreement with MRSDCI calculation. For comparison with calculations, all experimental momentum distributions in the illustrations in this paper have been divided by the corresponding pole strength.

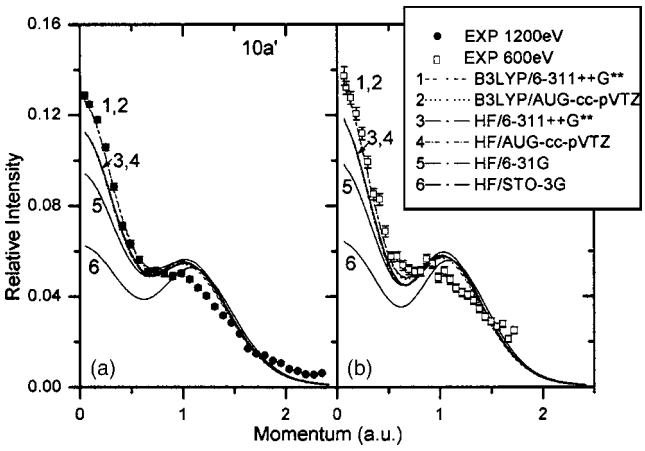

FIG. 2. Measured and calculated spherically averaged momentum profiles for the $10a'$ orbital of propene at impact energies of 1200 eV and 600 eV. All calculations have been folded with the experimental momentum resolution.

C. Outer valence orbital $2a''$, $10a'$, and $9a'$

The theoretical and experimental momentum profiles of the highest occupied molecular orbital $2a''$ have been discussed in Ref. 19, thus not presented here. A different impact energy is helpful for discussing some discrepancies between the experiment and the calculations, so the experiment was carried out at impact energies of 1200 eV and 600 eV. In this work, all the XMP were compared with the corresponding theoretical momentum profiles (TMP) at both impact energies. The slight difference of TMPs between 1200 eV and 600 eV is due to the changing of experimental momentum resolutions: the lower the impact energy, the higher is the momentum resolution. To reduce the excessive figures, only TMPs of 1200 eV are given at the following figures.

Figure 2 shows the XMPs of $10a'$ orbital compared with the DFT and HF calculations employing various basis sets as indicated by the legends. It can be seen that the DFT calculations (B3LYP/6-311++G** and B3LYP/AUG-cc-pVTZ) give the proper intensity in low-momentum region (curves 1 and 2), and all other calculations underestimate the experimental intensity in $p<0.8$ a.u. momentum region. In high-momentum region, although there is some discrepancy between XMPs and TMPs, TMPs well describe the observed intensity characteristics except the HF/STO-3G calculation (curve 6) in general.

The $9a'$ orbital is predominantly s-type as illustrated in Fig. 3. In general, the DFT and HF calculations with 6-311++G** and AUG-cc-pVTZ sets (curves 1–4) well reproduce the shape and intensity of the observed $9a'$ orbital momentum profiles. Among them, the DFT calculations (curves 1 and 2) describe XMPs slightly better than HF. However, though the theoretical calculations excellently agree with experiments, the discrepancy in $p<0.4$ a.u. region should not

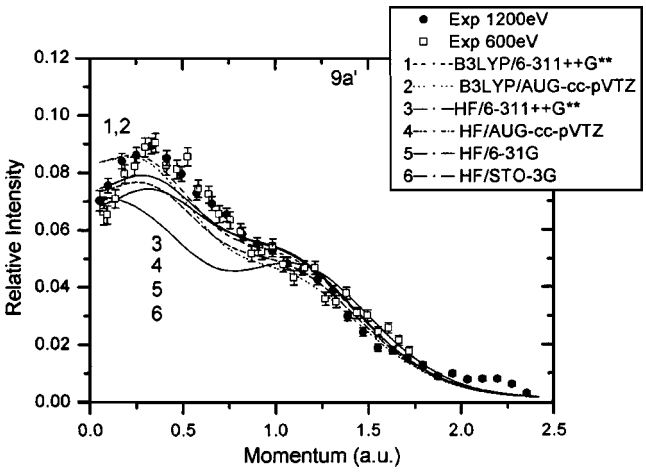

FIG. 3. Measured and calculated spherically averaged momentum profiles for the $9a'$ orbital of propene at impact energies of 1200 eV and 600 eV. All calculations have been folded with the experimental momentum resolution.

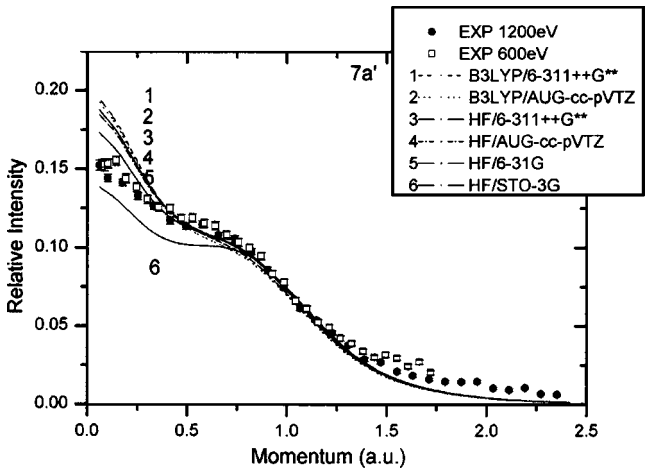

FIG. 5. Measured and calculated spherically averaged momentum profiles for the $7a'$ orbital of propene at impact energies of 1200 eV and 600 eV. All calculations have been folded with the experimental momentum resolution.

be neglected. It may be due to that there is some extent of the mixture of the *p*-type orbitals $8a'$ and $1a''$ in the XMPs since they are close spaced in the energy spectra.

D. Outer-valence orbital $8a'$, $1a''$, $7a'$ and their ordering

The difference of ionization potentials of $8a'$ and $1a''$ is only 0.52 eV which is beyond the experimental energy resolution, so a summed XMP was compared with corresponding calculations as shown in Fig. 4. Although the calculations predict the shape well, the discrepancy is obvious in the region <0.6 a.u. It is interesting to note that the calculations underestimate the observed intensity of orbital $8a'+1a''$, while overestimate that of $7a'$ as shown in Fig. 5, so it is reasonable to sum all XMPs to compare with calculations because they cannot be clearly separated in the binding energy spectra. As demonstrated in Fig. 6, a much better agreement is obtained by the summing up. However, some experimental intensity still remains unaccounted for the region around 0.8 a.u.

The ordering $8a'$, $1a''$ is disputant in previous literatures. References 6 and 8 give the order

$$\text{I:}\quad 9a' < 1a'' < 8a' < 7a',$$

while Ref. 9 proposed the following

$$\text{II:}\quad 9a' < 8a' < 1a'' < 7a'.$$

The difference between two sets assignment lies in the energy of $8a'$ and $1a''$. Although PES has a much higher energy resolution, for instance, FWHM of He I better than 30 meV, the PES experiment cannot, by itself, decide the relative ordering of the primary ionization energies.[9] The angle-resolved high energy resolution PES can determine orbital assignments by β parameter.[20] For EMS, although the energy resolution of the spectrometer in this work is 1.2 eV, it has its own unique power to identify orbitals. The momentum distributions of $9a'$, $8a'$, $1a''$, and $7a'$ are highly characteristic as shown in Figs. 3–5, so EMS should be able to provide some useful information for their ordering. Since $8a'$ and $1a''$ energy spectra overlap too much due to their smaller

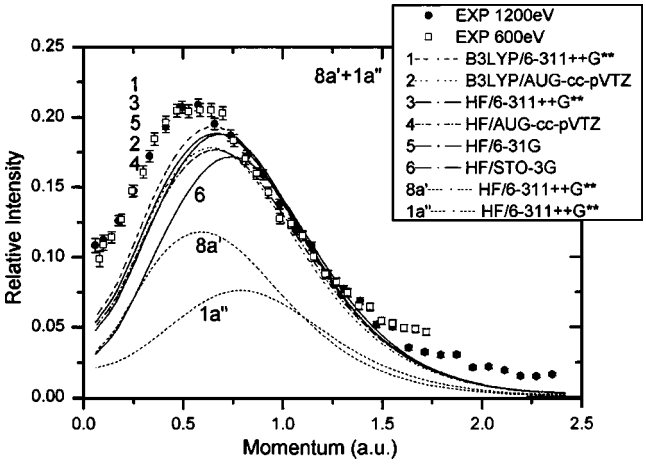

FIG. 4. Measured and calculated spherically averaged momentum profiles for the sum of $8a'$ and $1a''$ orbitals of propene at impact energies of 1200 eV and 600 eV. All calculations have been folded with the experimental momentum resolution.

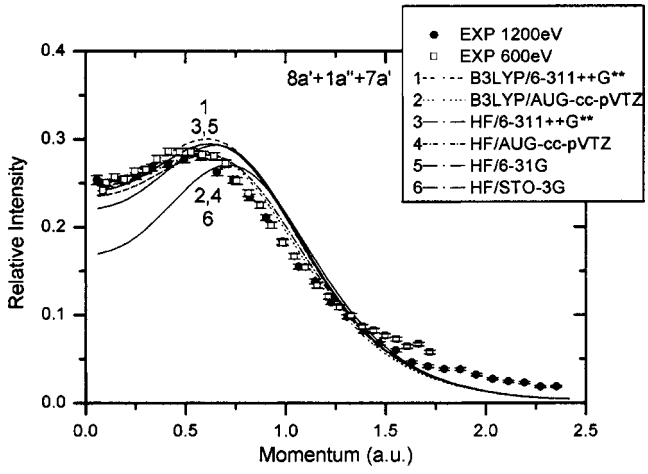

FIG. 6. Measured and calculated spherically averaged momentum profiles for the sum of $8a'$, $1a''$, and $7a'$ orbital of propene at impact energies of 1200 eV and 600 eV. All calculations have been folded with the experimental momentum resolution.

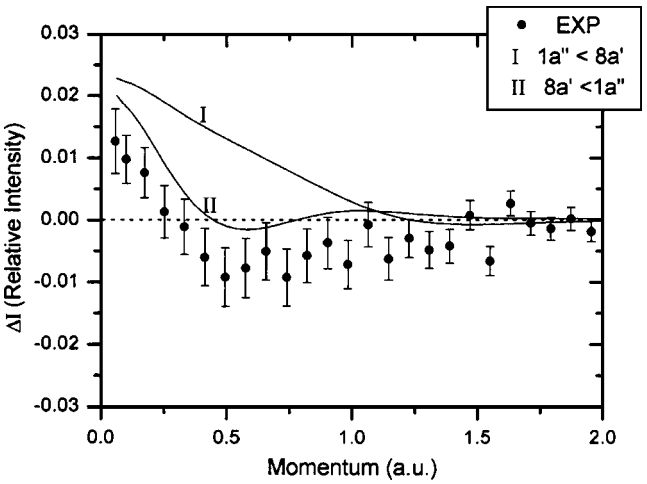

FIG. 7. Measured and calculated difference of momentum profiles between energy region 14.4 eV$<E<$14.8 eV and 14.8 eV$<E<$15.2 eV at an impact energy of 1200 eV plus binding energy. The calculation is at HF/6-311++G^{**} level and have been folded with the experimental momentum resolution. See text for details.

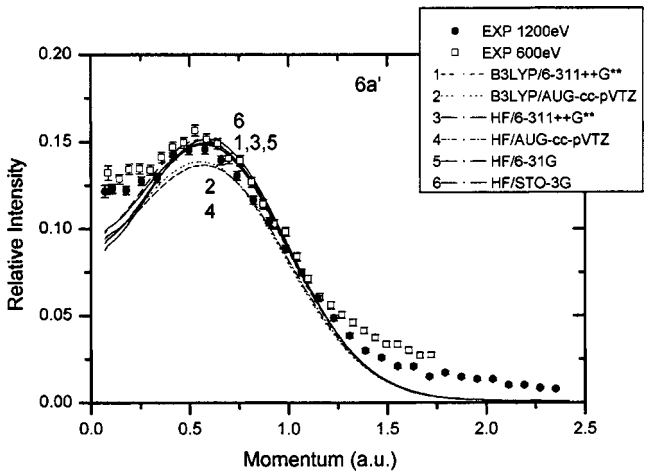

FIG. 8. Measured and calculated spherically averaged momentum profiles for the 6a' orbital of propene at impact energies of 1200 eV and 600 eV. All calculations have been folded with the experimental momentum resolution.

energy gap, there is deconvolution uncertainty. In consequence, we could not obtain proper experimental momentum profiles to compare with the theoretical one directly and respectively. An alternative approach must be taken to resolve this problem. If we cut two energy slices at 14.4–14.8 eV (defined as left) and 14.8–15.2 eV (right) in the map of Fig. 1, it is expected that there is a difference between the theoretical momentum profiles at the two energy slices due to the different ordering. To elucidate this issue clearly, we define

$$I(p)_{\text{left}} = \int_{14.4}^{14.8} \sum_i \rho_i(p) \frac{1}{\sqrt{2\pi} a_i} \exp\left(- \frac{(E-\varepsilon_i)^2}{2a_i^2} \right) dE,$$

$$I(p)_{\text{right}} = \int_{14.8}^{15.2} \sum_i \rho_i(p) \frac{1}{\sqrt{2\pi} a_i} \exp\left(- \frac{(E-\varepsilon_i)^2}{2a_i^2} \right) dE,$$

$$\Delta I(p)_{\text{the}} = I(p)_{\text{right}} - I(p)_{\text{left}}, \tag{8}$$

where $\rho_i(p)$ is the theoretical momentum profile (incorporated with experimental momentum resolution) of the ith orbital. Since the main contribution at this energy region is from orbitals 9a', 1a'', 8a', and 7a', other orbitals' contribution is not included in calculations. ε_i is the ionization potential of the ith orbital obtained from PES and $a_i = \text{FWHM}_i/(2\sqrt{\ln 4})$ (in this case, all FWHM_i equal 1.4 eV).

Correspondingly, the experimental data are given by

$$\Delta_{\text{expt}}(p) = \sum_{E=14.8}^{15.2} I_{\text{expt}}(E,p) - \sum_{E=14.4}^{14.8} I_{\text{expt}}(E,p), \tag{9}$$

where $I_{\text{expt}}(E,p)$ is the experimental intensity as shown in the map of Fig. 1 and the momentum p is related to ϕ by Eq. (1). As illustrated in Fig. 7, it is unanimous that the ordering of II described the experimental data better than I, though the calculation overestimates the experimental intensity in low-momentum region, so the correct order should be 9a' $<8a'<1a''<7a'$.

E. Inner-valence orbital 6a', 5a', and 4a'

The correlation effects in inner-valence orbitals are so severe that the measured pole strengths for primary ionizations of 6a', 5a', and 4a' by EMS are 0.75, 0.52, and 0.33, respectively. The peak corresponding to 6a' orbital is well resolved from the adjacent obitals in the energy spectra, as shown in Fig. 1(b). The experimental momentum distribution is presented in Fig. 8 together with the theoretical calculations. It can be seen that the six theoretical curves in this figure are divided into two groups. The curves 2 and 4 with AUG-cc-pVTZ basis sets are very similar in shape, while all other calculations (curves 1, 3, 5, and 6) produce almost same results even for the smallest set STO-3G. Since 6a' orbital is an inner-valence orbital, adding more polarized and diffusive terms to the basis set is unlikely to have significant influences on the calculational results. In general, all six calculations well describe the XMPs. However, one should see that XMPs turn up in the region $p<0.3$ a.u. and $p>1.1$ a.u. The turn-up at higher momentum is due to distorted wave effects because the inner-valence orbital is closer to the nucleus. The XMPs of other inner-valence orbitals 5a' and 4a' also show the similar turn-up at higher momentum, as illustrated in Figs. 9 and 10, respectively. With a lower impact energy, the distorted wave effects should be more pronounced. As Figs. 8–10 demonstrated, the turn-ups of 600 eV impact energy at high momentum become higher than that of 1200 eV. So the distorted wave effect qualitatively explains this discrepancy. However, the turn-up in the region $p<0.3$ a.u. in Fig. 8 still remains unaccountable. As Fig. 1 shows, the peak of 6a' is well resolved in the binding energy spectra, so it is unlikely due to the mixture of other primary peaks. A reasonable guess is that the turn-up in the region $p<0.3$ a.u. may be caused by the satellite lines because there are several satellite lines in this energy region according to MRSDCI calculations.[9]

In the binding energy spectra as shown by Fig. 1, peaks corresponding to the inner-valence orbitals 5a' and 4a' stand on a broad satellite band because the correlation effects are severe in this energy region. The XMPs of orbitals 5a' and

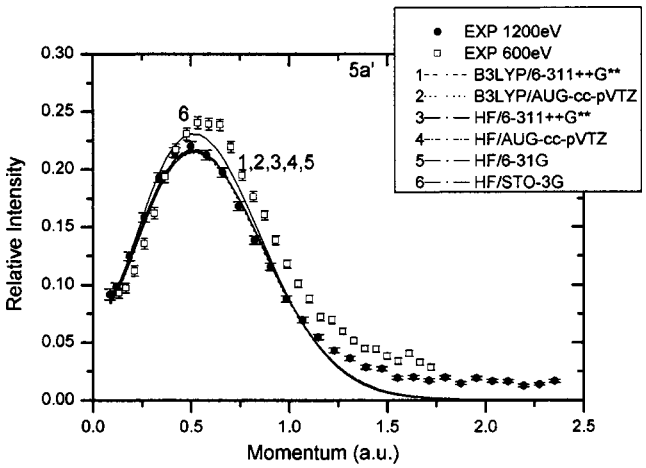

FIG. 9. Measured and calculated spherically averaged momentum profiles for the $5a'$ orbital of propene at impact energies of 1200 eV and 600 eV. All calculations have been folded with the experimental momentum resolution.

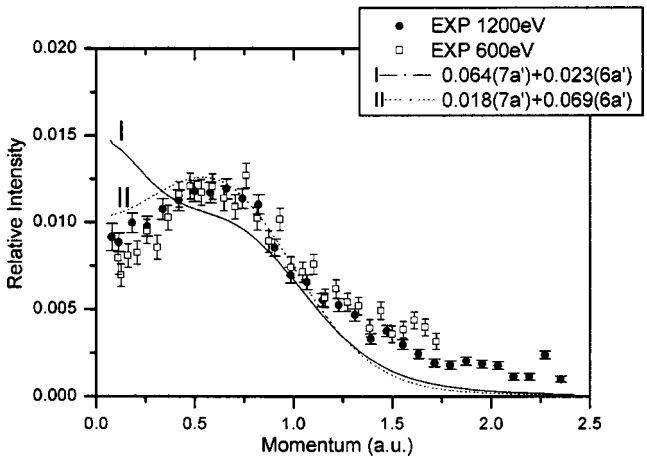

FIG. 11. Measured and calculated spherically averaged momentum profiles for the satellite line *a* at impact energies of 1200 eV and 600 eV. The calculation is at B3LYP/6-311++G* quality level.

$4a'$ and TMPs are compared in Figs. 9 and 10, respectively. All calculations almost produce identical results except HF/STO-3G method (curve 6), and, in general, well reproduce the experimental data. However, some discrepancies should not be neglected, especially in Fig. 10, because the agreement between TMPs and XMPs for inner-valence orbitals of small molecules is generally excellent. It is very likely that the deconvolution procedures did not well subtract the satellite lines contribution.

The XMP of satellite line indicated by *a* is shown in Fig. 11. It can be seen that this satellite line is predominantly *p* type. It has been established that satellite bands have the same momentum profile as the main configuration.[21] In addition, more recent measurements of argon satellite lines by a high-resolution EMS spectrometer also demonstrated this conclusion.[22] The MRSDCI calculations by Bawagan *et al.*[9] indicated that the correlation peak *a* is associated with at least two correlation states whose dominant configurations were $(8a')^{-1}(2a'')^{-1}(3a'')^{1}$ and $(10a')^{-1}(2a'')^{-1}(3a'')^{1}$ corresponding to binding root energies of 20.43 eV and 21.85 eV, respectively. The two correlation states borrow intensity from the ionization of two main orbitals: $(6a')^{-1}$ for 20.43 eV with pole strength of 0.023 and $(7a')^{-1}$ for 21.85 eV with 0.064, so the following combination of $6a'$ and $7a'$ was compared with XMP,

$$\text{I:}\quad 0.023(6a') + 0.064(7a').$$

As Fig. 11 shows, it could not well reproduce the XMP. The shape of calculations (curve I) is mainly *s* type, while XMPs are some matter of *p* type. The theoretical calculation method is at DFT with basis sets of B3LYP/6-311++G** level. However, if the following combination was taken, the agreement between theoretical calculations and XMP in shape was improved greatly,

$$\text{II:}\quad 0.069(6a') + 0.018(7a').$$

On the other hand, the experimental intensity is much higher than the calculated one. Only when dividing the experimental intensity by 2.0, could the calculations well describe it. So its pole strength is 0.17, i.e., $2.0\times(0.069+0.018)$. The discrepancy may be due to that there are some contributions from the adjacent primary orbitals, i.e., $6a'$ and $5a'$, which are predominant *p*-type orbitals. In addition, the energy of configuration $(10a')^{-1}(2a'')^{-1}(3a'')^{1}$ actually locates some far away from 20.3 eV, so its contribution in this region is much lower as theoretical calculations expected.

Figure 12 illustrates the momentum distribution of the summed satellite lines. It looks like some *s*-type orbital. Generally, many summed satellite lines with various characteristics will produce such momentum distributions, and even for outer-valence orbitals, if adding up them all, the summed experimental momentum distributions manifest a similar characteristic.[11,18,23]

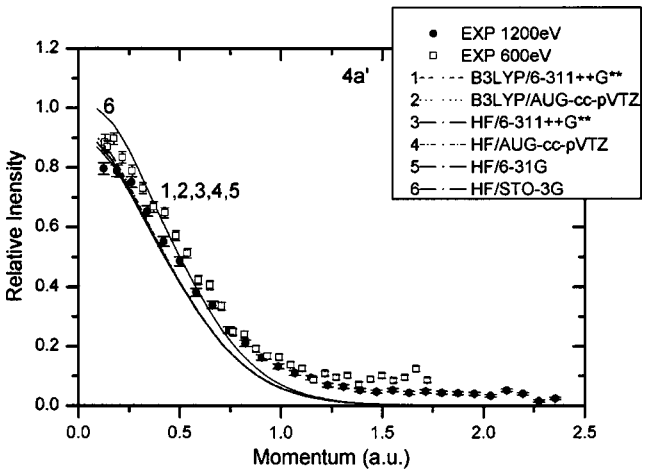

FIG. 10. Measured and calculated spherically averaged momentum profiles for the $4a'$ orbital of propene at impact energies of 1200 eV and 600 eV. All calculations have been folded with the experimental momentum resolution.

IV. SUMMARY

The experimental momentum profiles for full valence shell of propene have been obtained at impact energies of 1200 eV and 600 eV for the first time. The theoretical DFT and HF calculation based various basis sets are compared with the experimental momentum spectra. In general, the agreement between calculations and experiments is excel-

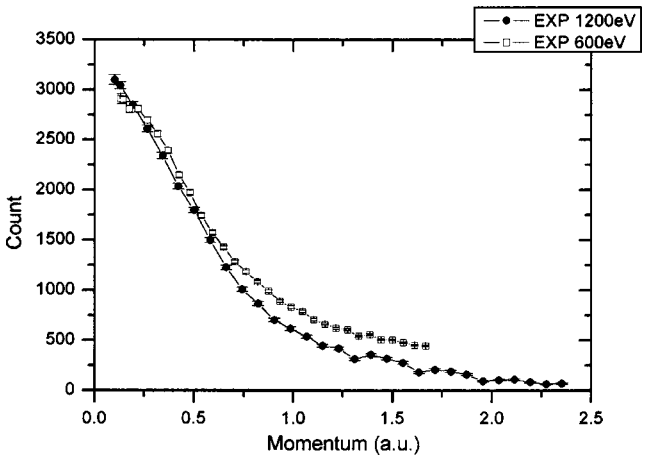

FIG. 12. Measured momentum profiles for the summed satellite lines at an impact energy of at impact energies of 1200 eV and 600 eV.

lent. For the outer-valence orbitals, the DFT calculations with basis sets 6-311++G^{**} and AUG-cc-pVTZ are slightly better than HF calculations on predicting the momentum distributions, especially in the low-momentum region.

Moreover, a difference analysis method presents an experimental support for the correct ordering of the orbital $8a'$ and $1a''$, i.e., $9a' < 8a' < 1a'' < 7a'$. Although the energy difference between $8a'$ and $1a''$ is beyond the EMS energy resolving power, EMS still can provide useful information for orbital assignment. Ordering of propene in this work provides a good example of the application of EMS on determining the similar indefinite ordering of molecular orbitals with small energy gaps.

ACKNOWLEDGMENTS

This project was supported by the National Natural Science Foundation of China under Grant Nos. 19854002, 19774037, and 10274040 and the Research Fund for the Doctoral Program of Higher Education under Grant No. 1999000327.

[1] E. McCarthy and E. Weigold, Rep. Prog. Phys. **54**, 789 (1991).
[2] M. A. Coplan, J. H. Moore, and J. P. Doering, Rev. Mod. Phys. **66**, 985 (1994).
[3] E. Weigold and I. E. McCarthy, *Electron Momentum Spectroscopy* (Kulwer Academic, New York, 1999).
[4] D. L. Cooper and N. L. Allan, J. Comput.-Aided Mol. Des. **3**, 253 (1989).
[5] D. L. Cooper, K. A. Mort, N. L. Allan, D. Kinchington, and C. McGuigan, J. Am. Chem. Soc. **115**, 12615 (1993).
[6] K. Kimura, S. Katsuwata, Y. Achiba, T. Yamazaki, and S. Iwata, *Handbook of HeI Photoelectron Spectra of Fundamental Organic Molecules* (Halsted, New York, 1981).
[7] G. Bieri, F. Burger, E. Heilbronner, and J. P. Maier, Helv. Chim. Acta **60**, 2213 (1977).
[8] C. Liegener, S. Svensson, and H. Agren, Chem. Phys. **179**, 313 (1994).
[9] A. D. O. Bawagan, S. J. Desjardins, R. Dailey, and E. R. Davidson, J. Chem. Phys. **107**, 11 (1997).
[10] X. J. Chen, L. X. Zhou, X. H. Zhang, X. F. Yin, C. K. Xu, X. Shan, Z. Wei, and K. Z. Xu, J. Chem. Phys. **120**, 7933 (2004).
[11] M. Takahashi, R. Ogino, and Y. Udagawa, Chem. Phys. Lett. **288**, 821 (1998).
[12] K. T. Leung and C. E. Brion, Chem. Phys. **95**, 241 (1985).
[13] A. Minchinton, J. P. D. Cook, and E. Weigold, Chem. Phys. Lett. **113**, 251 (1987).
[14] J. K. Deng, G. Q. Li, Y. He *et al.*, J. Chem. Phys. **114**, 882 (2001).
[15] P. Duffy, D. P. Chong, M. E. Casida, and D. R. Salahub, Phys. Rev. A **50**, 4704 (1994).
[16] J. N. Migdall, M. A. Coplan, D. S. Hench, J. H. Moore, J. A. Tossell, V. H. Smith, Jr., and J. W. Liu, Chem. Phys. **57**, 141 (1981).
[17] G. Fronzoni, G. DeAlti, P. Decleva, and A. Lisini, Chem. Phys. **195**, 171 (1995).
[18] O. Samardzic, M. J. Brunger, A. M. Grisogon, and E. Weigold, J. Phys. B **26**, 3921 (1993).
[19] C. G. Ning, X. G. Ren, J. K. Deng *et al.*, Chem. Phys. Lett. **402**, 175 (2005).
[20] M. N. Piancastelli, P. R. Keller, J. W. Taylor, F. A. Grimm, and T. A. Carlson, J. Am. Chem. Soc. **105**, 4235 (1983).
[21] I. E. McCarthy and E. Weigold, Phys. Rep., Phys. Lett. **27**, 275 (1976).
[22] M. J. Brunger, I. E. McCarthy, and E. Weigold, Phys. Rev. A **59**, 1245 (1999).
[23] M. Takahashi, K. Otsuka, and Y. Udagawa, Chem. Phys. **227**, 375 (1998).